Q. J. R. Meteorol. Soc. (2002), **128**, pp. 1847–1877

The impact of various potential-vorticity anomalies on multiple frontal cyclogenesis events

By DA-LIN ZHANG[1]*, WILLIAM Y. Y. CHENG[2] and JOHN R. GYAKUM[3]

[1]*University of Maryland College Park, USA*
[2]*Colorado State University, USA*
[3]*McGill University, Canada*

(Received 21 May 2001; revised 11 March 2002)

SUMMARY

The influences of various potential vorticity (PV) anomalies on multiple frontal cyclogenesis events are examined using 60 h simulations of a family of six frontal cyclones that developed over the western Atlantic between 0000 UTC 13 March and 1200 UTC 15 March 1992. The cyclogenesis events are characterized by pronounced low-level baroclinicity along a large-scale cold front moving over the warm ocean and by multiple propagating perturbations in the two PV rings on the cyclonic-shear side of an upper-level jet stream. It is found that the tracks of the frontal cyclones follow closely the distribution of the PV rings, whereas the cyclogenesis occurs in the cold-frontal zone, and in close proximity to the propagating PV perturbations in the central portion of an upper-level parent trough. A piecewise PV inversion reveals that the low-level thermal advection (or the bottom thermal anomaly) contributes the most to the depths of two major frontal cyclones, followed by latent-heat release and the upper-level PV anomalies, whereas the opposite order is true for the remaining four weaker frontal cyclones.

A series of sensitivity experiments is performed to test the impact of removing the upper-level PV anomalies individually, or collectively, on the development of a major frontal cyclone (MFC) as an initial-value problem. It is found that the MFC genesis and its final intensity depend on how much its track departs from the upper-level PV perturbations. Removing a PV anomaly associated with a major short-wave trough delays the MFC genesis by 18 h and weakens its final depth by 13 hPa. The largest departure occurs when two upstream PV anomalies are removed collectively, delaying the MFC genesis by 36 h and weakening its final depth by 21 hPa. It appears that the MFC genesis in the first 36 h depends more on the PV anomalies in an inner PV ring, whereas its subsequent development depends more on the PV reservoir in an outer PV ring.

It is shown that most of the frontal cyclones can still develop in the absence of diabatic heating, indicating the important role of dry dynamics in controlling the multiple frontal cyclogenesis events. However, the 'dry' MFC fails to form a closed isobar when the trough-related PV anomaly is removed. The associated PV inversion and sensitivity simulation results suggest that even though the low-level thermal advection plays an important role in deepening the frontal cyclones, it is the upper-level PV anomalies that provide the necessary forcing for its amplification and the frontal cyclogenesis.

It is concluded that the upper-level propagating *multiple* PV anomalies play a major role in triggering, but a secondary role in determining the final depth of the *multiple* frontal cyclones. It is the subsequent growth of the bottom thermal anomaly that accounts for most of the final depth of the frontal cyclones.

KEYWORDS: Numerical weather prediction Oceanic storms Potential-vorticity inversion

1. INTRODUCTION

Although there have been considerable advances in understanding the structures and behaviour of synoptic-scale extratropical cyclones (see the comprehensive reviews given in Newton and Holopainen (1990) and Shapiro and Gronas (1999)), our knowledge of frontal or secondary cyclogenesis† and its behaviour in relation to larger-scale flows is rather limited. So far, only a few frontal-cyclogenesis studies have been conducted owing to the lack of high-resolution meteorological observations. However, growing attention has recently been paid to the frontal cyclogenesis phenomenon since the conduct of the Fronts and Atlantic Storm-Track EXperiment (FASTEX, Snyder 1996; Joly *et al.* 1997).

* Corresponding author: Department of Meteorology, University of Maryland College Park, Maryland, 20742, USA. e-mail: dalin@atmos.umd.edu

† Frontal or secondary cyclogenesis is defined herein as taking place in the lowest 200–500 hPa with a diameter of 500–2000 km on the trailing cold front of a 'parent' cyclone.

Previous studies revealed that frontal cyclones are distinct from their synoptic-scale counterparts not only in spatial and temporal scales but sometimes in intensifying mechanisms. For example, most synoptic-scale cyclones are baroclinically driven and modulated by latent-heat release (Davis *et al.* 1993; Huo *et al.* 1996). In contrast, frontal cyclogenesis may result from latent-heat release and subsequent growth in the frontal zone (Joly and Thorpe 1990), the growth of a low-level warm band with uniform potential vorticity (PV) (Schär and Davies 1990), the interaction with an upper-level PV cut-off (Thorncroft and Hoskins 1990), the growth of low-level PV anomalies under the influence of frontogenetic deformation (Bishop and Thorpe 1994), the propagation of upper-level PV anomalies across the low-level frontal zone (Hoskins *et al.* 1985) or *a combination of the above processes* (Zhang *et al.* 1999a,b). As compared with the synoptic-scale counterpart, there appears to be no general agreement on the dominant role of any particular parameter in triggering frontal cyclogenesis and in determining the structures and the final intensity of frontal cyclones (Parker 1998). In fact, a large variety of secondary cyclones with different structures and intensifying mechanisms have been sampled during FASTEX (see Baehr *et al.* 1999; Joly *et al.* 1999).

In addition, some secondary cyclogenesis appears to be sensitive to slight changes in the model initial conditions and the model physics representations (Lapenta and Seaman 1992; Wang and Zhang 2000), since the pertinent mesoscale circulations are often too small to be detected by the conventional network. Because of its small horizontal scale and shallow vertical depth, frontal cyclogenesis also tends to be more significantly influenced by the bottom boundary conditions than synoptic-scale counterparts, such as surface friction (i.e. land vs. ocean), and surface latent- and sensible-heat fluxes (see Carrera *et al.* 1999; Zhang *et al.* 1999b). Thus, more case-studies are needed to investigate different processes in early cyclogenesis and to gain insight into their relative importance in determining the behaviour and final intensity of frontal cyclones.

The objectives of the present study are to (i) examine multiple frontal cyclogenesis events and their behaviour in relation to large-scale flows and upper-level PV anomalies; and (ii) quantify the relative contributions of diabatic heating, upper-level PV anomalies and low-level baroclinicity to frontal cyclogenesis. The objectives will be achieved using 60 h simulations of a family of six frontal cyclones which occurred over the western Atlantic between 0000 UTC 13 March and 1200 UTC 15 March 1992. Zhang *et al.* (1999a) have shown that the Pennsylvania State University/National Center for Atmospheric Research (PSU/NCAR) mesoscale model reproduces the development, tracks and intensity of the six frontal cyclones, using a full-physics package with a fine-mesh grid size of 30 km, as verified against the Canadian Meteorological Centre analysis and satellite observations.

For ease of reference in the subsequent discussions, we display in Fig. 1 three surface maps of the frontal-cyclone family that are taken from the model initial time, and 24 and 48 h simulations, valid at 0000 UTC 13, 14 and 15 March 1992 (henceforth 13/00-00, 14/00-24, 15/00-48), respectively. The three periods represent the pre-cyclogenesis, incipient and mature stages of the oceanic storm. There are three frontal cyclones at 15/00-48: the northern (NFC), major (MFC) and southern (SFC) ones, as denoted by N, M, and S, respectively (Fig. 1(c)). They are initiated in the cold sector as a pressure trough and then amplified in the frontal zone that is originally associated with a parent cyclone (P) to the north (Figs. 1(a) and (b)); each successive family member is formed to the south-west of its predecessor (Bjerknes and Solberg 1922). They exhibit a depth of 100–300 hPa in the lower troposphere (see Zhang *et al.* 1999a) with diameters ranging from 500 to 1100 km (as estimated by the last closed isobar). Of particular significance is that the MFC undergoes explosive deepening (at a rate

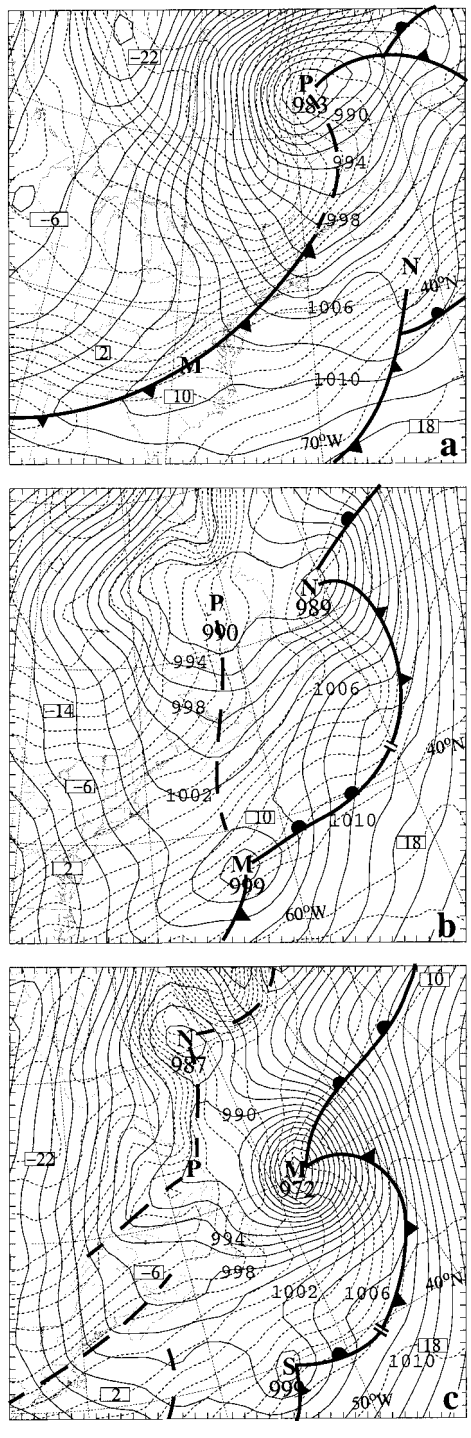

Figure 1. Sea-level pressure (solid, every 2 hPa) and surface temperature (dashed, every 2 degC) from (a) the model initial time (i.e. 00 UTC 13 March 1992); (b) 24 h simulation (i.e. 00 UTC 14 March 1992) and (c) 48 h simulation (i.e. 00 UTC 15 March 1992). P, M, N, and S denote the centres of the parent, major, northern, and southern frontal cyclones, respectively.

of 44 hPa (42 h)$^{-1}$) and absorbs the low-level circulations of the parent cyclone and the NFC after 15/00-48. Lemaître *et al.* (1999) and Bouniol *et al.* (1999) have studied a case of rapid frontal cyclogenesis, occurring during FASTEX, with a deepening rate as large as 54 hPa (24 h)$^{-1}$. Joly *et al.* (1999) showed that most of the FASTEX cyclones deepened at rates greater than 6 hPa (6 h)$^{-1}$.

In a subsequent study, Zhang *et al.* (1999b) showed that dry dynamics determines the initiation and track of the frontal cyclones and accounts for a large percentage of the deepening of the MFC and NFC. A similar conclusion has also been obtained by Mallet *et al.* (1999) for a case of rapid frontal cyclogenesis during FASTEX. In the present study, the 13–15 March 1992 frontal cyclogenesis attributions will be examined in the context of Ertel's PV, following Davis and Emanuel (1991) and Huo *et al.* (1999a,b). Because of its attractive conservative property and invertibility principle, the PV concept has recently been successfully used to gain insight into the influence of upper-level PV anomalies on the development of extratropical cyclones (Davis and Emanuel 1991; Huo *et al.* 1999a,b) and frontal cyclones (Demirtas and Thorpe 1999; Fehlmann and Davies 1999). However, it is still unclear to what extent the frontal cyclogenesis is determined by latent-heat release, upper-level PV anomalies and other dynamical processes as mentioned above.

The next section shows the structures and evolution of upper-level PV anomalies and large-scale flows in relation to the surface frontal cyclones. More attention will be given to the evolution of the MFC owing to its rapidly deepening characteristics. The MFC forms its first closed isobar at 13/18-18 in the absence of local diabatic heating, as it moves over the warm Gulf Stream water (Zhang *et al.* 1999a). Section 3 quantifies the relative contributions of different PV anomalies to the genesis and final intensity of the frontal cyclones through the piecewise PV inversion. Section 4 examines the roles of multiple upper-level PV anomalies in triggering the frontal cyclogenesis by removing these anomalies individually, or collectively, and then treating them as an initial-value problem. Section 5 shows the relative importance of upper- versus low-level dynamical processes in the frontal cyclogenesis in the context of dry dynamics. Some concluding remarks are given in the final section.

2. Potential-vorticity analysis

Figure 2 shows the 300 and 900 hPa PV structures at the model initial time (i.e. 13/00). There is little low-level PV in the frontal cyclogenesis region. An area of positive PV is concentrated to the north in association with the parent cyclone (cf. Figs. 1(a) and 2). By comparison, the upper troposphere is characterized by *a PV ring on the cyclonic-shear side of a jet stream* with extremely small PV in the central weak-flow region. We will see in section 4 that the local PV maxima, H_1, H_2 and H_3, in the ring produce different degrees of influences on the development of the MFC, NFC and SFC. In particular, the MFC (NFC) is located downstream of a short-wave trough with PV peaking at H_1 (H_0), and an intense PV centre H_2 (H_3) farther upstream; their central values exceed 6 PV units (1 PVU $= 10^{-6}$ K kg^{-1}m^{2}s^{-1}). If a typical value of 2 PVU is used to define the dynamic tropopause, the PV perturbations are indicative of local tropopause depressions, and the PV ring represents the interface between the polar air mass in the central weak-flow region and the tropical air mass outside.

By 14/00-24, the short-wave trough has lost its identity, owing to the decrease in its curvature vorticity, as it moves through the near-straight jet stream (cf. Figs. 2 and 3(a)). However, because its associated PV perturbation H_1 is being advected rapidly toward the MFC where the lower-tropospheric static stability (over the ocean) is weak, it begins

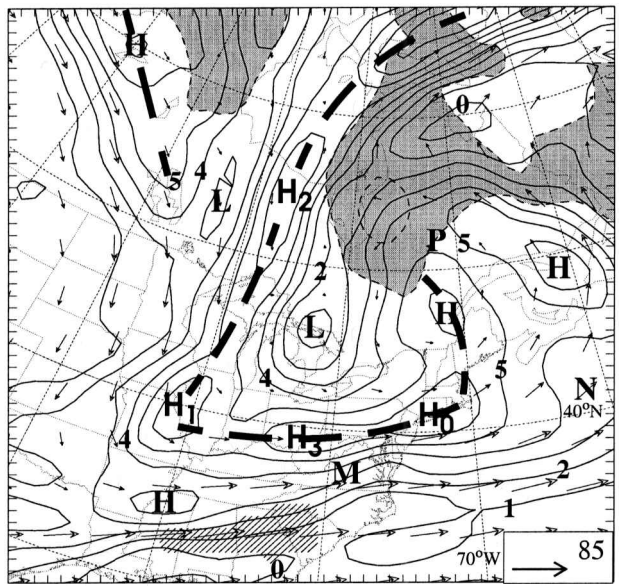

Figure 2. Distribution of 300 hPa potential vorticity (PV, solid) and 900 hPa PV (dashed and shaded) at intervals of 1 PV unit (1 PVU = 10^{-6} K kg^{-1}m^{2}s^{-1}), superposed with 300 hPa wind vectors at the model initial time (i.e. 00 UTC 13 March 1992). H_1, H_2, and H_3 (H_0) denote the local PV maxima at 300 hPa that have potential influence on the development of the major frontal cyclone (northern frontal cyclone). H and L indicate the centres of other local PV maxima and minima, respectively. Thick dashed line denotes the axis of the PV ring and hatched areas represent the 300 hPa jet-streak core. Inset indicates the scale of horizontal wind (m s^{-1}).

to influence the surface MFC perturbation, as will be shown in section 5. Of interest is that another PV ring forms outside the first one due partly to the rapid advection of a PV anomaly from the north-west on the cyclonic-shear side of the jet stream (cf. Figs. 2 and 3(a)) and partly to the poleward retreat of the first PV ring (henceforth the outer and inner rings, respectively). It appears that the PV reservoir in the outer ring begins to influence the MFC development at this time, but more significantly after 14/12-36, based on Figs. 3–5 and 9–12. We acknowledge that this outer PV ring was not discussed in our previous studies (i.e. in Zhang *et al.* 1999a,b), because it is less evident below the 300 hPa level. The 6-day track of the MFC, shown in Zhang *et al.* (1999a), resembles closely the distribution of the two PV rings, indicating the possible role of their induced flows in steering this frontal cyclone as well as the other members of the cyclone family. Similarly, H_3 has been rapidly advected north-eastward to influence the NFC. As the surface systems deepen, significant low-level PV begins to develop in the vicinity of the MFC and NFC, which is indicative of latent-heat release (see Boyle and Bosart 1986; Whitaker *et al.* 1988; Davis and Emanuel 1991; Huo *et al.* 1996).

A vertical cross-section through the MFC shows weak dry descent of stratospheric PV in the inner PV ring, but little evidence of descent in the outer ring. The two PV perturbations, denoted by the 1 PVU contour, have penetrated to 500 hPa (Fig. 3(b)). In contrast, the diabatically generated PV during the previous 6 h resides completely within cloudy regions, as represented by the area with relative humidity >90%. Of importance is that this low-level PV perturbation is almost 'locked' with the leading PV perturbation in the outer ring throughout the MFC's deepening stage. Ahead of the PV perturbation and to the north of the MFC, the dynamic tropopause is elevated partly

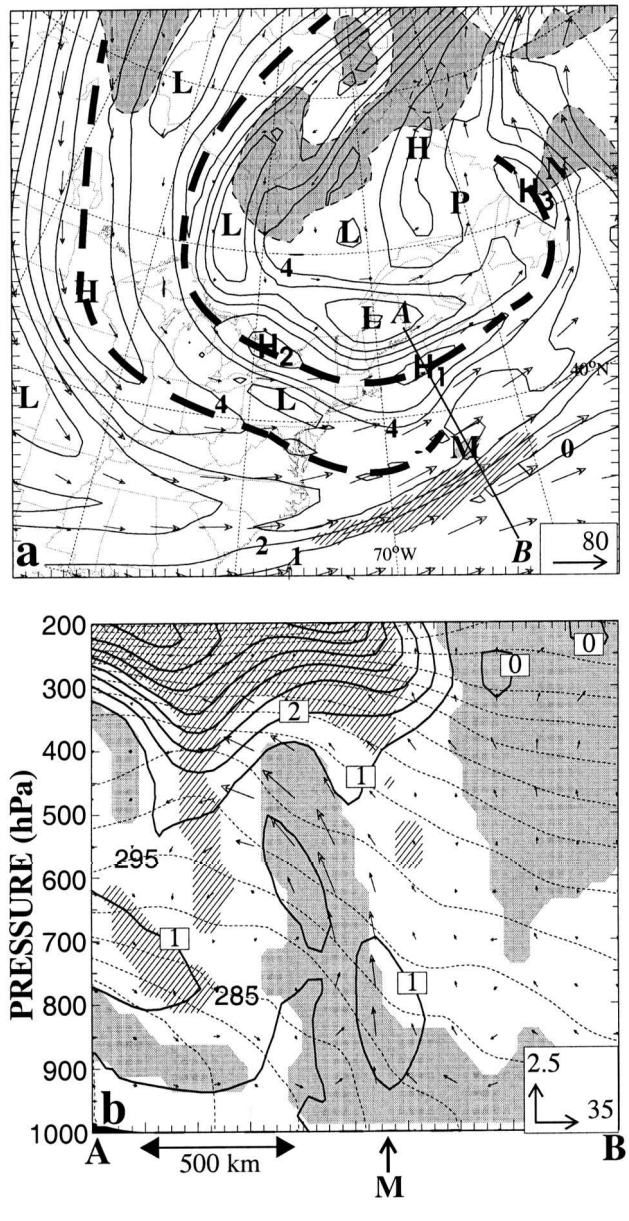

Figure 3. (a) Distribution of 300 hPa potential vorticity (PV, solid) and 900 hPa PV (dashed and shaded) at intervals of 1 PV unit (1 PVU = 10^{-6} K kg^{-1}m^{2}s^{-1}), superposed with 300 hPa wind vectors at 00 UTC 14 March 1992. H_1, H_2 and H_3 denote the local PV maxima at 300 hPa that have potential influence on the development of the major frontal cyclone. Thick dashed line denotes the axis of the PV ring and hatched areas represent the 300 hPa jet-streak core. (b) Vertical cross-section of PV (solid) at intervals of 1 PVU and potential temperature (dashed) at intervals of 5 K, superposed with along-plane flow vectors, along line AB given in (a). Hatching and shading in (b) denote relative humidity <30% and >90%, respectively. Inset indicates the scale of vertical motion (Pa s^{-1}) and horizontal wind (m s^{-1}).

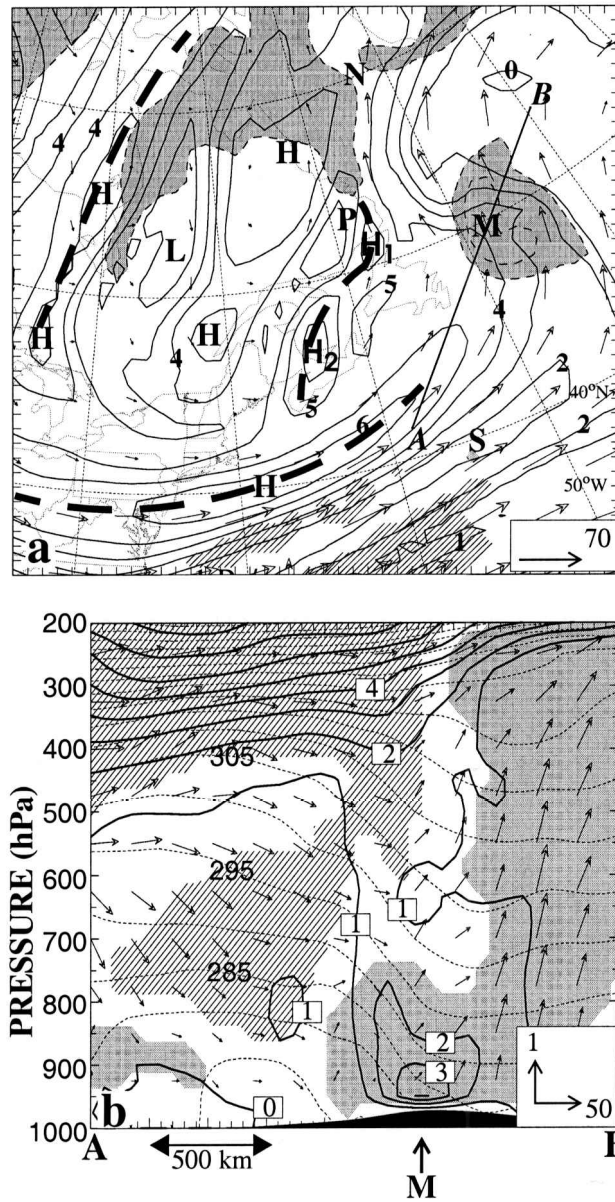

Figure 4. As in Fig. 3 but for 00 UTC 15 March 1992.

by the erosion of lower PV that occurs between the two rings and partly by slantwise upward advection above the warm-frontal zone (cf. Figs. 1 and 3).

By 15/00-48, the MFC has propagated to the exit region of the jet stream or into the region with more influence from the upper-level ridge (Fig. 4). The PV reservoir in the outer ring appears to dominate the MFC, as the latter departs farther away from the inner ring, and it now exhibits the dry descent of the stratospheric air behind. During this mature stage, a low-level 'comma-shaped' PV perturbation, exceeding 3 PVU, is generated near the MFC centre. Like the MFC and NFC, the SFC and remaining

frontal cyclones are initiated as PV perturbations in the outer-ring approach (Fig. 4(a)). For the SFC, its associated latent heating gives rise to a small region of low-level PV (cf. Figs. 1(b) and 4(a)), which could be inferred from the active cloud systems visible in the satellite images (see Fig. 12 in Zhang *et al.* 1999a).

It is evident that *(a) all the frontal cyclones are initiated on the cyclonic-shear side of the upper-level jet stream but equatorward of a PV ring, and (b) their initial genesis occurs in the trailing frontal zone of the parent cyclone and over the central portion of the large-scale trough*. Clearly, the influences of various PV perturbations in the two PV rings on the different frontal cyclones are another unique aspect of this case-study.

3. Cyclogenesis attributions

In this section, we use the piecewise PV inversion technique developed by Davis and Emanuel (1991) to quantify the effects of the above-mentioned PV perturbations on the surface development. To this end, the total PV field is first partitioned into a background PV and its departures (or anomalies), and the associated mass and wind perturbations are then inverted to estimate the relative contributions of different PV anomalies to the surface cyclogenesis. In the present case, the background PV field is obtained from the time mean between 1200 UTC 10 March and 1200 UTC 17 March 1992 plus the first Fourier harmonic of this time series; the latter is added to filter out the domain-scale signals from the PV anomalies. To provide meaningful cyclogenesis attributions, the PV anomalies are classified, according to Davis and Emanuel (1991) and Huo *et al.* (1999a), into four groups: (i) upper-level dry PV anomalies (in the two PV rings) with stratospheric origin (Q_d); (ii) low-level moist PV anomalies produced by latent-heat release (Q_h); (iii) effective bottom potential-temperature anomalies (θ_{eff}) that combine the bottom boundary θ perturbations and low-level interior PV; and (iv) the remaining PV anomalies (Q_r). Because Q_r is dominated mainly by upper-level ridges, it is here combined with Q_d as one upper-level PV anomaly, following Huo *et al.* (1999a). Huo *et al.* (1999a) showed how these PV anomalies could interact with each other vertically and laterally.

Tables 1–4 show the time series of area-averaged 1000 hPa geopotential-height perturbations, centred at the frontal cyclones, that are inverted at 12 h intervals from the above-mentioned PV anomalies. It is evident that the total height perturbation associated with the MFC increases with time, e.g. from −187 m at 13/12-12 to −526 m at 15/12-60 (see Table 1), which is consistent with the deepening of the storm. Of interest is that the largest contribution to the MFC's depth comes from θ_{eff}, with an average value of 44.3%, followed by Q_h with an average value of 40.3%. Their absolute contributions also increase during the rapid MFC genesis (i.e. from 13/12-12 to 15/00-48) as a consequence of the positive feedback between latent-heat release, and pressure falls induced by various PV anomalies. The relative contribution from θ_{eff} reaches as high as 55.8% at 14/00-24 during the most rapid deepening phase. The relative contribution from Q_h peaks at 52.3% at 14/12-36, after which time less moisture is available for condensation as the MFC moves over colder water. It should be noted that while the θ_{eff} contribution is pronounced, it could not be materialized without the external forcing of Q_d+Q_r and Q_h; this will be shown in section 5. The upper-level contribution becomes more significant in both absolute and relative values only at 15/12-60 when the MFC absorbs the NFC and the parent cyclonic circulations.

Vertical cross-sections of the inverted geopotential height, given in Fig. 5, show the relationship between the MFC and the various grouped PV anomalies. First, note the location, size, and intensity of three distinct anomaly groups in the vertical: Q_d+Q_r

TABLE 1. THE MAGNITUDES (dam) AND THE RELATIVE CONTRIBUTIONS (%) TO THE 1000 hPa GEOPOTENTIAL HEIGHT INVERTED FROM THE UPPER-LEVEL DRY-PLUS-RESIDUAL POTENTIAL VORTICITY (PV) ANOMALIES (Q_d+Q_r), LOW-LEVEL MOIST PV ANOMALY (Q_h), AND EFFECTIVE BOTTOM POTENTIAL-TEMPERATURE ANOMALY (θ_{eff}). THEY ARE OBTAINED BY AVERAGING OVER AN AREA OF 360 km × 360 km CENTRED AT THE MAJOR FRONTAL CYCLONE.

Day/hour	Q_d+Q_r dam (%)	Q_h dam (%)	θ_{eff} dam (%)	Total dam
13/00	−3.9 (19.6)	−5.7 (28.6)	−10.3 (51.8)	−19.9
13/12	−4.0 (21.4)	−5.5 (29.4)	−9.2 (49.2)	−18.7
14/00	1.0 (−4.5)	−10.9 (48.7)	−12.5 (55.8)	−22.4
14/12	−1.9 (5.2)	−19.0 (52.3)	−15.4 (42.5)	−36.3
15/00	−7.8 (15.2)	−21.5 (41.8)	−22.1 (43.0)	−51.4
15/12	−18.7 (35.6)	−21.5 (40.8)	−12.4 (23.6)	−52.6

TABLE 2. AS IN TABLE 1 BUT FOR THE NORTHERN FRONTAL CYCLONE

Day/hour	Q_d+Q_r dam (%)	Q_h dam (%)	θ_{eff} dam (%)	Total dam
13/00	−0.1 (0.4)	−7.1 (31.0)	−15.7 (68.6)	−22.9
13/12	9.3 (−36.0)	−11.8 (45.7)	−23.3 (90.3)	−25.8
14/00	6.5 (−19.0)	−12.2 (35.6)	−28.6 (83.4)	−34.3
14/12	3.8 (−13.1)	−15.0 (51.9)	−17.7 (61.2)	−28.9
15/00	3.6 (−13.2)	−13.1 (48.0)	−17.8 (65.2)	−27.3

TABLE 3. AS IN TABLE 1 BUT FOR THE SOUTHERN FRONTAL CYCLONE

Day/hour	Q_d+Q_r dam (%)	Q_h dam (%)	θ_{eff} dam (%)	Total dam
14/12	−6.0 (28.8)	−7.9 (38.0)	−6.9 (33.2)	−20.8
15/00	−13.0 (46.9)	−7.5 (27.1)	−7.2 (26.0)	−27.7
15/12	−14.3 (44.5)	−8.2 (25.5)	−9.6 (30.0)	−32.1

TABLE 4. AS IN TABLE 1 BUT FOR L_1, L_2, AND L_3 (SEE TEXT) AT 12 UTC 15 MARCH 1992

Trough	Q_d+Q_r dam (%)	Q_h dam (%)	θ_{eff} dam (%)	Total dam
L_1	−19.3 (67.7)	−6.9 (24.2)	−2.3 (8.1)	−28.5
L_2	−14.8 (68.2)	−4.8 (22.1)	−2.1 (9.7)	−21.7
L_3	−9.1 (44.8)	−3.2 (15.8)	−8.0 (39.4)	−20.3

above 500 hPa, Q_h in the 600–1000 hPa layer, and θ_{eff} at the bottom boundary. Their induced height falls all increase from 14/00-24 to 15/00-48 as the MFC deepens. More pronounced increases appear in θ_{eff} and Q_h. Second, the influence of Q_d+Q_r is widespread and throughout the troposphere, with evident ridge and trough structures. However, their influences decrease downward as a result of stronger static stability in the lower troposphere, namely, having limited penetration depth in the cold sector (Hoskins *et al.* 1985). Nevertheless, their influences are much deeper at 15/00-48 owing to the increased amplitude of Q_d+Q_r (cf. Figs. 5(a) and (b)). Third, the influence of H_1 on the MFC appears to be more pronounced than the outer-ring induced at 14/00-24;

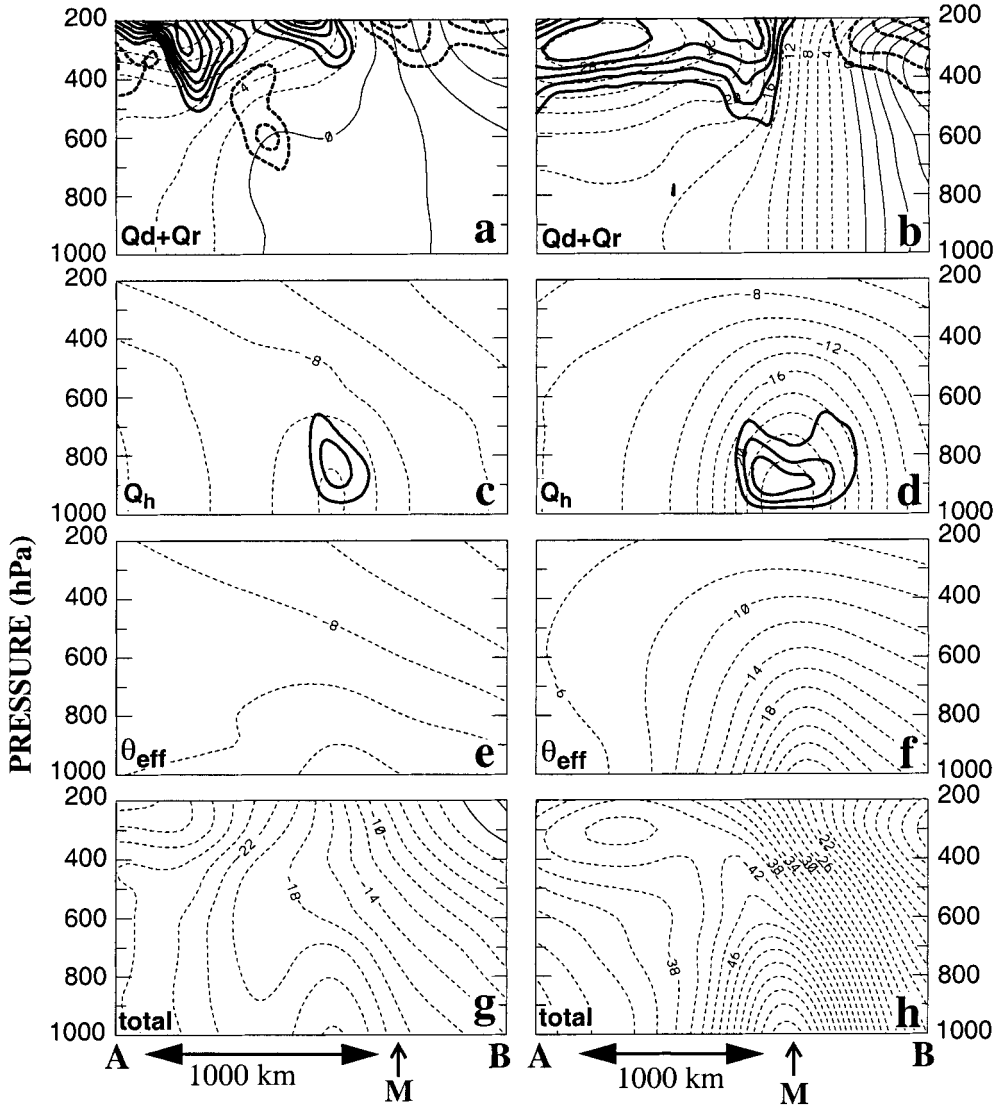

Figure 5. Vertical cross-section of the inverted geopotential-height perturbations (thin lines, every 2 dam) from (a) and (b): upper-level potential vorticity (PV) anomalies (Q_d+Q_r); (c) and (d): low-level moist PV anomaly (Q_h); (e) and (f): effective bottom potential-temperature anomaly (Q_{eff}); (g) and (h): total perturbations, superposed with their corresponding PV anomalies (thick lines, every 0.5 PV units (1 PVU $= 10^{-6}$ K kg^{-1}m^{2}s^{-1})). Solid (dashed) is positive (negative) with the zero contour suppressed. Left and right panels are obtained at 00 UTC 14 March and 00 UTC 15 March 1992 along line AB in Figs. 3(a) and 4(a), respectively.

its northward departure is consistent with the weak positive height change (i.e. +10 m) at the MFC centre at this time (see Table 1).

Note that the above-mentioned cyclogenesis attributions depict well a combination of what is implied by the theoretical impact studies of the upper-level PV anomalies (Figs. 5(a) and (b)) by Thorncroft and Hoskins (1990), the latent-heat release in the frontal zone (Figs. 5(c) and (d)) by Joly and Thorpe (1990), and the low-level thermal perturbations in the vicinity of a baroclinic zone (Figs. 5(e) and (f)) by Schär and Davies (1990). The sum of the inverted height perturbations shows a rearward-tilted lower

pressure pattern associated with the MFC in the lower half of the troposphere (Fig. 5(h)). During the mature stage, the MFC has a surface circulation of about 800 km in diameter that is embedded in the parent cyclone. These inverted height structures are similar to those of deviation heights shown in Zhang *et al.* (1999a, see Figs. 15 and 16 therein).

In contrast, the NFC develops in an environment that differs from that of the MFC in terms of the upper-level influences (see Figs. 2–4). For example, the height falls induced by Q_d+Q_r are mostly positive (see Table 2), except at the model initial time. Thus, the upper-level PV anomalies do not seem to be favourable for the NFC genesis after its formation. This could be attributed *partly to the dominant negative forcing from a large-scale ridge ahead during its late development stage, and partly to the lack of intense positive PV anomalies in its adjacent area* (see Figs. 2–4). Stronger static stability to the north relative to the MFC could also be an unfavourable factor. All this appears to explain partly why the NFC fails to intensify into a robust system. Apparently, it is θ_{eff} and Q_h that mostly assist the NFC development after 13/12-12; on average, they contribute respective values of 73.7% and 42.5% to its depth (Table 2). Of significance is that the θ_{eff} contribution reaches as high as 90% during the most rapid deepening stage in the first 12 h, indicating the importance of the low-level thermal perturbations in the NFC development. Of course, this does not imply that the upper-level PV perturbations have little impact on the NFC genesis. As shown in Zhang *et al.* (1999a), the NFC genesis corresponds well to a small trough in the upper troposphere during the first 12 h (see Fig. 3 therein). This trough (with a PV perturbation H_0 upstream) must have played some role in triggering the NFC genesis. Once its cyclonic circulation is established, the NFC could intensify via the θ_{eff} and Q_h contributions.

Because the SFC is triggered far away from the large-scale ridge system to the east, Q_d+Q_r associated with a PV perturbation in the outer ring (see Fig. 14(b) in Zhang *et al.* 1999a) contributes markedly to its deepening (see Table 3). The upper-level contribution ranges from 28.8% at the incipient stage to 46.9% at the mature stage, while Q_h and θ_{eff} account almost equally for the remaining contributions to the SFC's depth.

At the end of the 60 h integration, the model reproduces three surface frontal troughs during their incipient stage to the south-west of the SFC (see Fig. 11 in Zhang *et al.* 1999a). For completeness, the inverted results are given in Table 4, which shows the significant contributions of Q_d+Q_r (associated with PV perturbations in the outer ring) to the three systems' depth, like the SFC. They range from about 68% for the two leading frontal troughs (i.e. L_1 and L_2) to 44.8% for a third trough (i.e. L_3) at the south-west corner. This is again due to the reduced influence away from the large-scale ridge to the east, as compared with their three predecessors at this time. We speculate that the θ_{eff} contributions for L_1, L_2, L_3 and the SFC would increase with time, as occurred with the MFC and NFC, if they continued to deepen as they moved north-eastward.

The above results reveal that the bottom anomaly θ_{eff} and latent-heat release Q_h help deepen the MFC, NFC and SFC. Although the contributions of upper-level PV anomalies are relatively small (during the intensifying stages), they appear to account at least for triggering the genesis of most frontal cyclones in the present case.

4. Influence of upper-level PV anomalies on the frontal cyclogenesis

In this section, we attempt to determine which PV anomaly (i.e. H_1, H_2 or H_3) has the most significant influence on the frontal cyclogenesis. This can be done by removing the associated PV anomaly in the upper troposphere from the control initial conditions, and then examining its impact on the surface development via 60 h sensitivity integrations. For this purpose, the piecewise PV inversion is used again to invert

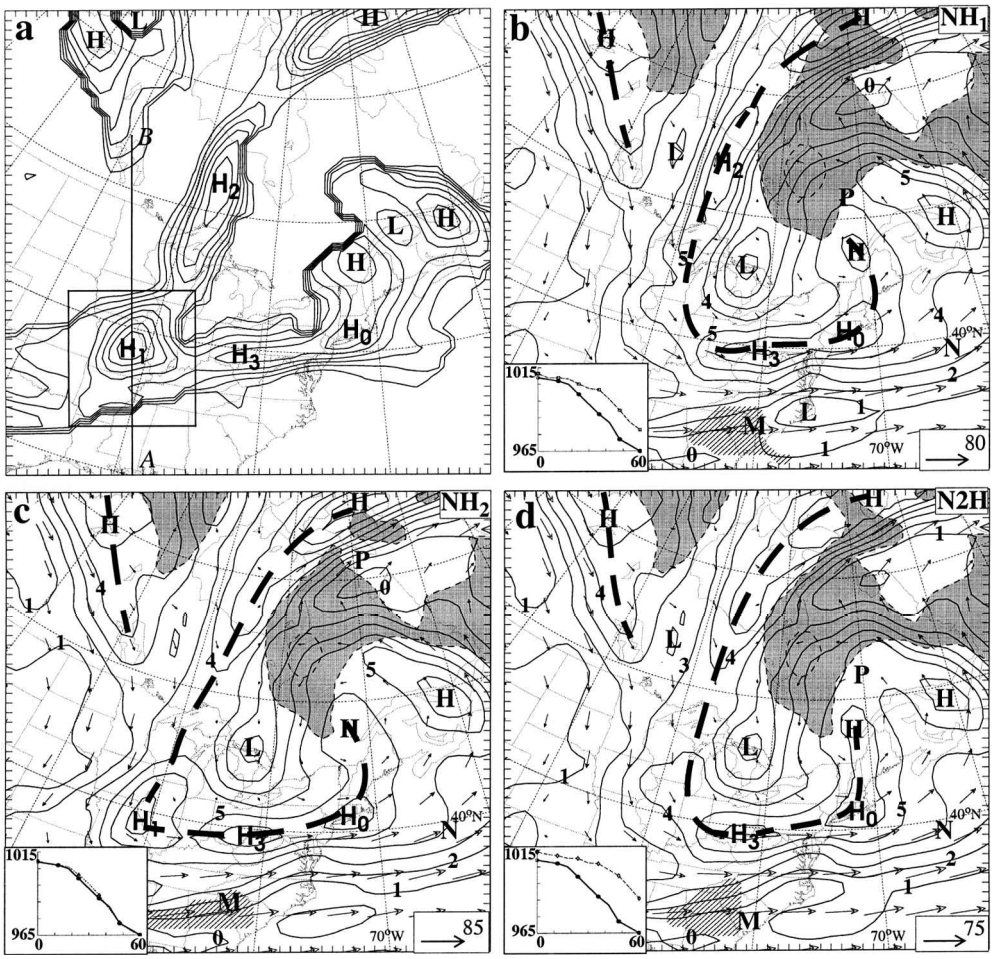

Figure 6. As in Fig. 2 but for (a) potential vorticity (PV) anomalies (every 0.5 PV unit (1 PVU = 10^{-6} K kg^{-1}m^{2}s^{-1}) starting from 0.5 PVU) that are obtained by subtracting its background and first Fourier harmonic (see section 3); (b) experiment NH_1; (c) NH_2; and (d) N2H. Line AB in (a) shows the locations of the cross-sections used in Fig. 8, and the box enclosing H_1 represents the area from which the PV anomaly is removed. In (b)–(d), the central pressure traces as a function of the model time are included for each sensitivity experiment, as compared with that in experiment CTL. See Table 5 for details of experiments.

each upper-level PV anomaly and the pertinent balanced wind and mass fields are then removed from the control initial conditions (see Huo *et al.* 1999a,b for more details). A similar approach has been used by Demirtas and Thorpe (1999) and Fehlmann and Davies (1999) to examine the influence of upper-level PV perturbations on the surface development. Figure 6(a) shows an example of the 300 hPa PV anomalies at 13/12-00 with a box enclosing the PV anomaly (H_1) to be removed. Note that the centres of the peak PV anomalies depart slightly from those of the PV perturbations (cf. Figs. 6(a) and 2) owing to the spatial distribution of local PV maxima in the background field being subtracted. Nevertheless, because of their proximities in physical location, we still refer to these PV perturbations (i.e. H_1, H_2, and H_3) as PV anomalies. We have attempted to remove PV anomalies in the outer PV ring at 13/00, 13/12 and 14/00, but with no success, due to their strong relationships with the upper-level jet stream. Thus, four

TABLE 5. EXPERIMENTAL DESIGN

Experiment	Description
CTL	The control simulation with full physics
NH_1	PV anomaly H_1 is removed from the CTL initial conditions
NH_2	PV anomaly H_2 is removed from the CTL initial conditions
NH_3	PV anomaly H_3 is removed from the CTL initial conditions
N2H	PV anomalies H_1 and H_2 are removed from the CTL initial conditions
DRY	Same as experiment CTL except that diabatic heating is turned off
NH_1D	Same as experiment NH1 except that diabatic heating is turned off

sensitivity experiments, as listed in Table 5, are conducted using the results presented in the preceding section as a control run (experiment CTL).

Figures 6(b)–(d) and 7 show the effectiveness of removing individually, or collectively, the upper-level PV anomalies. (Results associated with experiment NH_3 are not shown because the impact of removing H_3 is relatively small.) One can see that the upper-level local PV peaks associated with H_1, H_2, and H_1+H_2 are completely absent after the removal (cf. Figs. 2 and 6(b)–(d)). However, their nearby PV structures are slightly altered, because the influence of a PV anomaly acts in three dimensions throughout the domain. Of importance is that removal of H_1, H_2, and H_1+H_2 results in local higher pressures in the lower troposphere over the cold sector (cf. Figs. 1(a) and 7(a)–(c)), since removing a positive PV anomaly is equivalent to adding some air mass with anticyclonic vorticity in a vertical column. Moreover, owing to its close proximity to the MFC, removing H_1 (experiment NH_1) weakens significantly its associated pressure trough in the frontal zone (cf. Figs. 1(a) and 7(a) and (c)). Likewise, removing H_2 (experiment NH_2) produces a pronounced influence on the parent cyclone and the pressure structure nearby. Most significantly, when both H_1 and H_2 are removed simultaneously (experiment N2H), the MFC is displaced markedly southward such that it is located slightly *on the anticyclonic side* of the upper-level jet stream. As will be seen later, this is unfavourable for surface development owing to its increased distance from the upper-level PV reservoir (Figs. 6(d) and 7(c)). Nonetheless, removing these PV anomalies does affect the local, but only a little the synoptic-scale, morphology of the steering flow, and it does not seem to affect notably the structure and intensity of the NFC at the model initial time.

As an example of the removed mass- and wind-field magnitudes, Fig. 8 shows vertical cross-sections of the wind and mass fields that are inverted from the PV anomaly associated with H_1; similarly for H_2. These wind and mass perturbations are exactly the differences between experiments CTL and NH_1, and they are, as expected, more pronounced at the upper levels. The associated height deficit, exceeding 240 m, peaks near 300 hPa with the maximum cyclonic wind of 20 m s^{-1}, while the corresponding cooling, greater than 6 degC, is maximized near 500 hPa. With the height deficit removed, the (Q_d+Q_r)-induced perturbations, similar to those given in Figs. 5(a) and (b), could be eliminated or substantially reduced. This height deficit is hydrostatically related to the weak warming above and marked cooling below, and it is in approximate gradient-wind balance with the horizontal winds.

Because of the initial southward displacement of the parent cold front, all the tracks of the MFC begin at a distance of about 300 km to the south of the control one. However, this departure decreases sharply with time in experiment NH_2, and becomes extremely small after 14/00-24 (Fig. 9). In contrast, this departure only decreases slightly in experiment NH_1 during the first 24 h integration, and changes little during the second 24 h. On the other hand, when both PV anomalies are removed (i.e. H_1+H_2), the

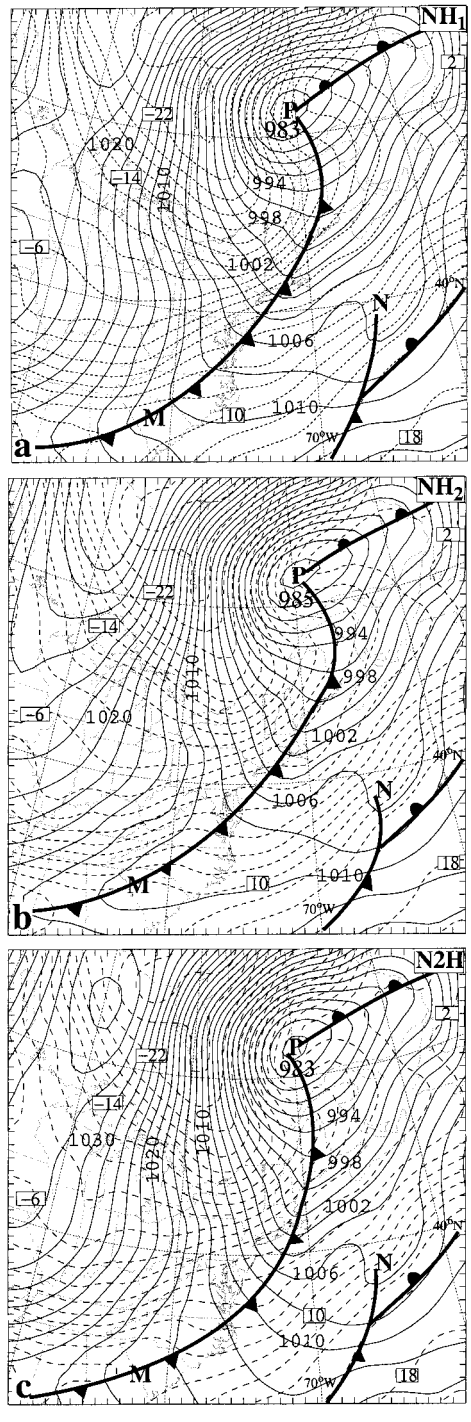

Figure 7. As in Fig. 1(a) but for experiments (a) NH_1; (b) NH_2; (c) N2H. See Table 5.

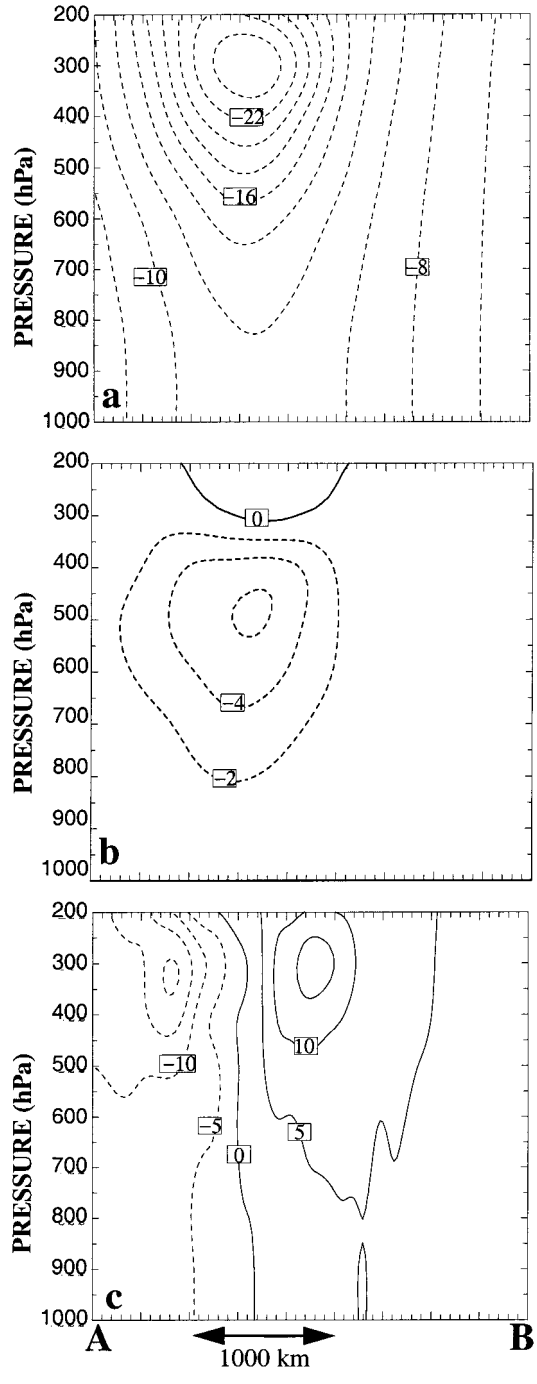

Figure 8. Vertical cross-section of (a) geopotential-height anomaly at intervals of 2 dam; (b) temperature anomaly at intervals of 2 degC; and (c) cross-sectional normal wind at intervals of 5 m s^{-1} with positive (negative) values representing the flow into (out of) the page. They are inverted from the PV anomaly H_I at 00 UTC 13 March 1992 and taken along AB in Fig. 6(a).

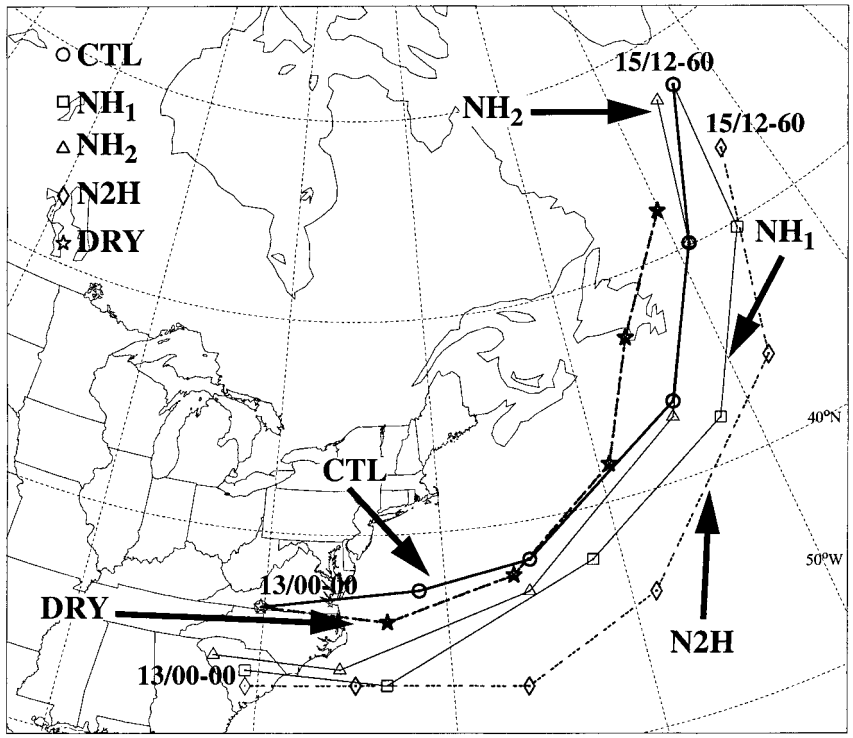

Figure 9. The simulated tracks of the major frontal cyclone between 13/00-00 (00 UTC 13 March 1992) and 15/12-60 (12 UTC 15 March 1992), labelled 12 hourly, from experiments CTL, NH_1, NH_2, N2H and DRY (see Table 5). Latitudes and longitudes are given every 10°.

MFC's track tends to depart in a more outward direction from the control one, probably resulting from the initial displacement to the anticyclonic side of the jet stream and the influence of the outer PV ring. As will be seen later (see Fig. 13), the outward departure in track reduces the influence of the upper-level PV reservoir in the inner ring on the MFC genesis during the first 36 h integration. Nevertheless, the departures between the sensitivity and control tracks decrease after 15/00-48, suggesting a more important role being played by the outer PV ring in determining the MFC track. Moreover, despite the marked departures, all the tracks follow an 'arc-shaped' trajectory, confirming again the importance of the PV rings (i.e. their induced flows) in steering the propagation of the frontal cyclones (Fig. 9).

The simulated time series of the MFC's central pressure are qualitatively consistent with the results of the tracks, i.e. mainly determined by the degree of the upper-level influence (see Figs. 10 and 13). Specifically, removing H_2 slows the MFC genesis during the incipient stage, but produces little impact on its final intensity, since H_1 and the outer PV ring appear to determine more significantly the MFC development during its life cycle (see Figs. 10, 11(b), and 12(b)). By comparison, removal of H_1 delays the genesis and weakens substantially the final intensity of the MFC. Only a weak trough is formed by 14/00-24, as compared with a distinct closed low in experiment CTL (cf. Figs. 1(b) and 11(a)). The first closed isobar associated with the MFC does not appear until 14/12-36, namely, a delay of cyclogenesis by 18 h. Its final central pressure at 15/12-60 is 978 hPa, which is 13 hPa weaker than the control simulation (Fig. 10(a)). Notwithstanding the weak pressure deficit, the MFC still experiences an

'explosive deepening' during the final 24 h, according to the definition of Sanders and Gyakum (1980); it occurs at a rate of 1 hPa h^{-1}. Note, though, that most of the central pressure drops are caused by their movement into the lower pressures of the parent cyclone, including the FASTEX cyclones listed by Joly *et al.* (1999). For instance, the MFC in NH_1 deepens by 17 hPa from 14/00-24 to 15/00-48, but its central pressure at 48 h is merely 6 hPa deeper than the outermost closed isobar (cf. Figs. 11(a) and 12(a)). As mentioned by Zhang *et al.* (1999a), this represents one of the distinct characteristics of frontal cyclones compared with their synoptic-scale counterparts.

While removing H_2 has little impact on the development of the MFC, removal of both H_1 and H_2 (i.e. experiment N2H) produces not only a marked delay in cyclogenesis but also a much reduced intensity. In particular, this frontal cyclone shows little evidence of intensification at 14/00-24 (Fig. 11(c)), and merely a deep trough at 15/00-48 (Fig. 12(c)). Its first closed isobar does not form until 15/08-54, namely, a delay of genesis by 36 h, at which time the system has moved to the unfavourable ridge area. The final central pressure of the MFC is 986 hPa, which is 21 hPa weaker than the control simulation (Fig. 10).

To help understand why the MFC deepens in NH_2 at a rate similar to that in CTL but behaves differently in other sensitivity simulations, Fig. 13 shows the relationship between the surface development and its distance from upper-level PV perturbations. Note first that the PV anomaly being removed in each run does not reappear later on as a distinct entity. While the PV anomalies could be removed successfully, new PV anomalies may be dynamically generated in the altered environment. Furthermore, the lack of lateral interactions between the removed and existing PV anomalies, as discussed in Hakim *et al.* (1996) and Huo *et al.* (1999a), could affect significantly the phase relationship between the upper- and lower-level disturbances. For example, replacing H_2 by a cold column tends to displace H_1 and its associated trough southward, while its removed cyclonic vorticity would slow the eastward progression of H_1 (cf. Figs. 3 and 13(b)) due to vortex–vortex interaction (see Huo *et al.* 1999a for more details). Removing H_2 has a slight impact on the MFC, because it is H_1 that accounts more for its first 24 h genesis and the outer PV ring that becomes more important during its final 24 h intensification.

In contrast, removing H_1 accelerates the eastward movement of H_2 but slows that of the MFC (cf. Figs. 3 and 13(a)). At 14/00-24, the MFC is located far away from H_2 and other PV anomalies, due partly to the absence of H_1 and partly to its initial southward displacement from the inner PV ring. Thus, little upper-level forcing is available for triggering the MFC genesis at this time (see Figs. 6(b) and 13(a)). More rapid deepening of the MFC occurs after the 36 h integration (see Fig. 10(a)) as the outer PV ring begins to influence its development. When H_1 and H_2 are both removed (experiment N2H), no new PV perturbations are generated in the PV ring. The MFC experiences the weakest development due to its marked departure in track from the inner PV ring (cf. Figs. 11–13). Nevertheless, it deepens at a rate similar to that in experiment NH_1 after the 36 h integration, due clearly to the influence of the PV reservoir in the outer PV ring.

By comparison, the NFC develops more favourably in experiments NH_1 and N2H, and its circulation is more robust than that in CTL due to the suppression of the MFC (see Zhang *et al.* 1999b for the related discussion). In the context of PV, the weakening of the MFC allows the bottom thermal anomaly θ_{eff} to play a more important role in the NFC genesis. The NFC attains a central pressure of 981 (971) hPa in experiment NH_1 (N2H) at 15/00-48, which is 5 (13) hPa deeper than the control one (cf. Figs. 1(c) and 12). In all of the sensitivity experiments, the SFC fails to emerge. But, several

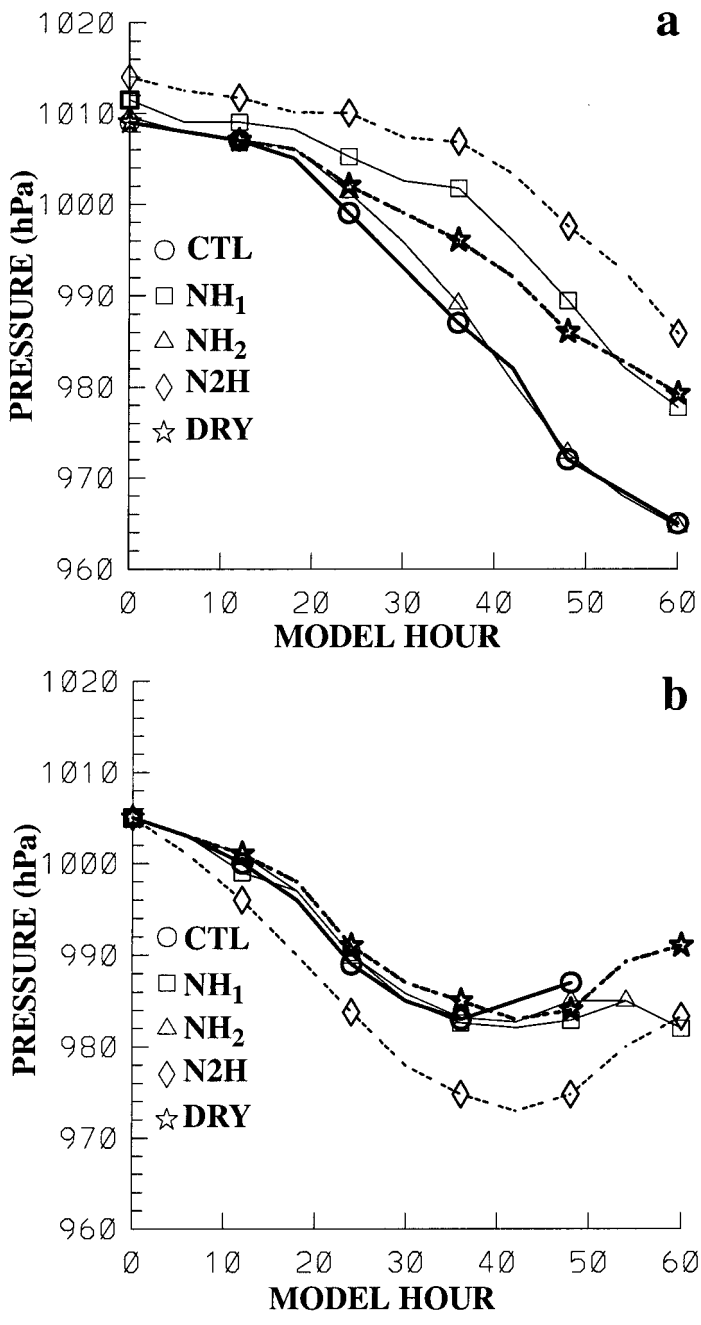

Figure 10. The central pressure traces of (a) the major frontal cyclone, and (b) the northern frontal cyclone from experiments CTL, NH_1, NH_2, N2H and DRY (see Table 5).

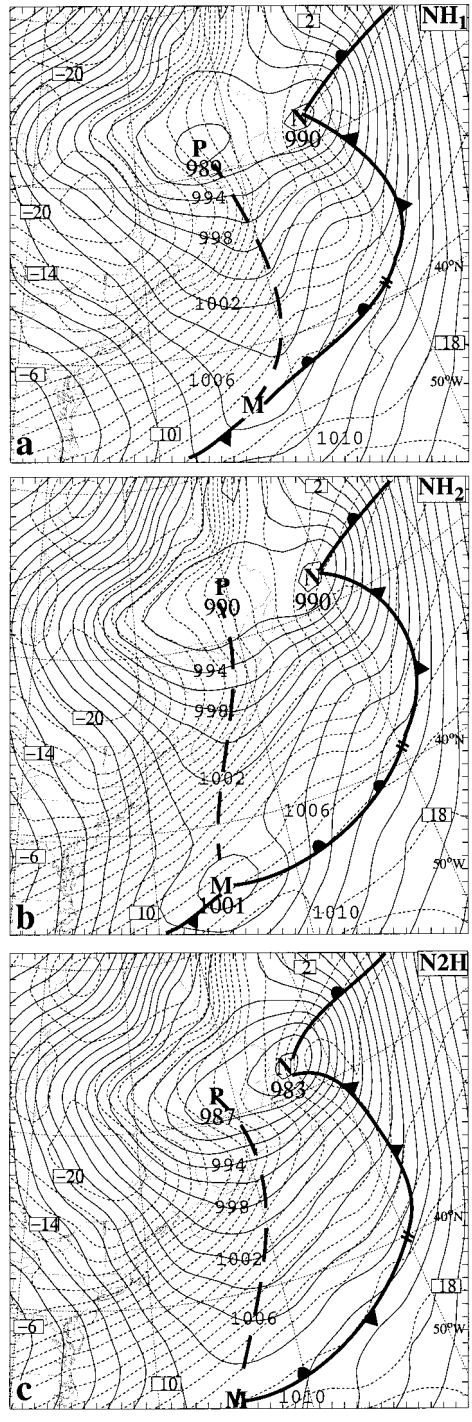

Figure 11. As in Fig. 1(b) but for experiments (a) NH_1; (b) NH_2; and (c) N2H at 00 UTC 14 March 1992 (see Table 5).

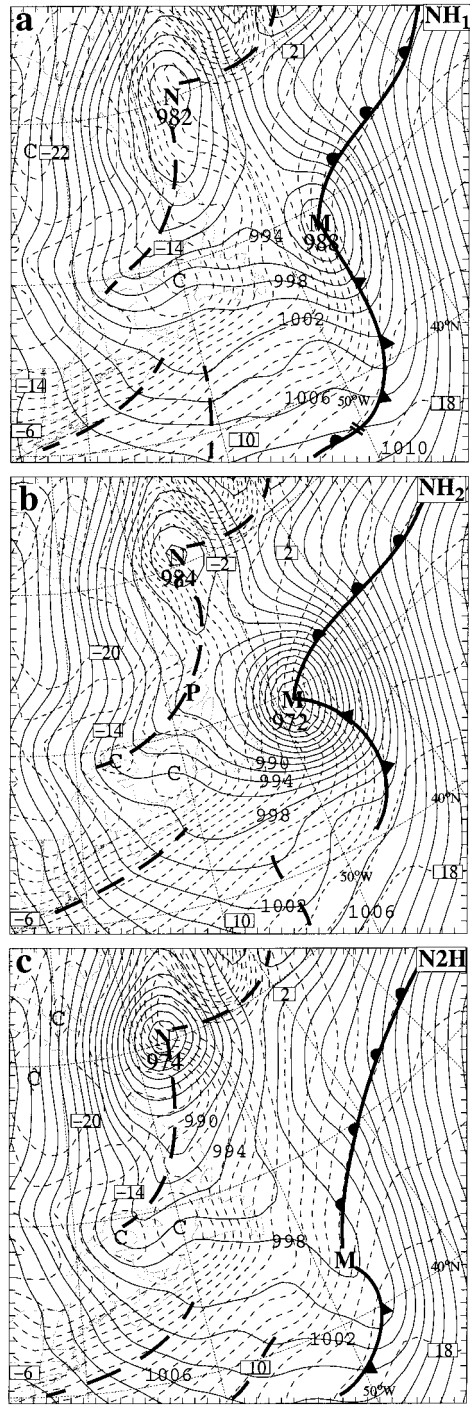

Figure 12. As in Fig. 1(c) but for experiments (a) NH_1; (b) NH_2; and (c) N2H at 00 UTC 15 March 1992 (see Table 5).

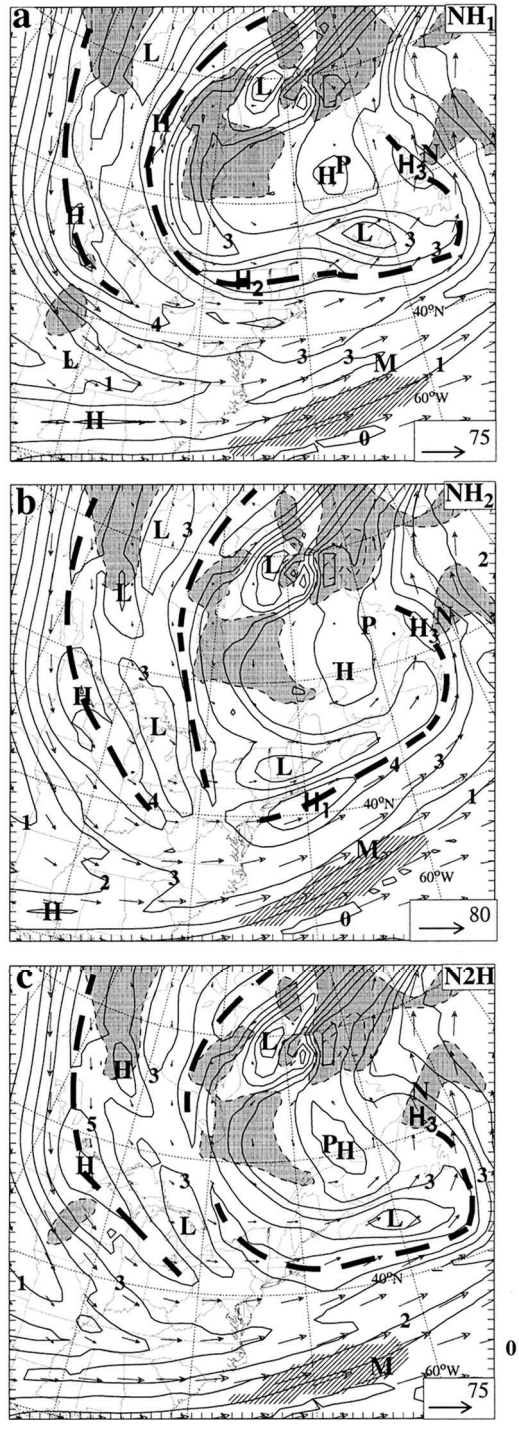

Figure 13. As in Fig. 2 but for experiments (a) NH_1; (b) NH_2; and (c) N2H at 00 UTC 14 March 1992 (see Table 5).

troughs in sea-level pressure are evident to the south-east of the MFC near the end of the 60 h integration (not shown), which are similar to those seen in experiment CTL. Again, they could be attributed to the multiple propagating perturbations in the outer PV ring.

5. Adiabatic dynamics

Since the MFC and NFC could still develop in the absence of diabatic heating (Zhang *et al.* 1999b; see Fig. 14(a) herein), some large-scale adiabatic processes must determine the genesis and movement of the frontal cyclones. Thus, it is desirable to investigate the impact of the multiple PV anomalies on the frontal cyclogenesis just using the numerical experiments in which latent-heat release is excluded. Without the diabatic heating, the cyclogenesis attributions could be significantly simplified. That is, we only need to consider the effects of *the upper-level (Q_d+Q_r) and the bottom (θ_{eff}) dry PV anomalies* on the frontal cyclogenesis.

(*a*) *Cyclogenesis attributions*

Figure 15 shows the 300 hPa PV structures from experiment DRY at 14/00-24, since this is the critical time in the triggering of the MFC by PV anomalies in the two upper-level PV rings. These PV structures are qualitatively similar to those in CTL, albeit slightly weaker and with fewer perturbations (cf. Figs. 15 and 3(a)). Apparently, the MFC genesis can take place in the absence of diabatic heating due partly to its location close to the PV perturbation H_1 in the first 36 h integration, and partly to the reduced static stability over the underlying warm water of the Gulf Stream (see Zhang *et al.* 1999a,b). The subsequent MFC development is closely related to the PV reservoir in the outer ring (see Fig. 4(a)), thereby leading to the continuous deepening of the frontal cyclone (i.e. from 1002 hPa at 14/00-24 to 986 hPa at 15/00-48; see Figs. 10(a) and 14(a)).

The dry cyclogenesis attributions associated with the MFC are given in Table 6, which shows the growing contributions from the upper- and low-level PV anomalies. They are similar to those in experiment CTL and consistent with the continued deepening of the dry cyclone. The relative contribution of Q_d+Q_r ranges from 25.5% at 13/12-12 to 46.7% at 15/12-60, with the remaining relative contribution by θ_{eff}. On average, Q_d+Q_r and θ_{eff} contribute 30.9% and 69.1% to the MFC's depth, respectively. This result confirms that obtained from experiment CTL, namely, θ_{eff} (or the low-level thermal advection) has dominant contributions to the MFC development. It is also in agreement with the conclusion obtained from the Zwack and Okossi (1986) vorticity budget calculations that the upper-level vorticity advection provides the necessary forcing for triggering and tracking the frontal cyclones, whereas the low-level thermal advection accounts for a large portion of the total deepening (see Zhang *et al.* 1999b). The same is true for the NFC (not shown). This appears to differ from the intensifying mechanisms of typical synoptic-scale cyclogenesis (e.g. Kuo and Reed 1988; Lupo *et al.* 1992; Reed *et al.* 1994; Huo *et al.* 1996), in which differential vorticity advection often dominates the rapid-deepening phase.

Vertical cross-sections of the inverted height anomalies through the MFC at the mature stage resemble in structure, but differ in magnitude and relative importance, from those in experiment CTL (cf. Figs. 16 and 5). In spite of its smaller amplitude, the upper-level PV anomaly (mostly associated with H_1) could still induce a negative height perturbation in a deep vertical column (Fig. 16(a)). It is evident that the θ_{eff}-induced height perturbation dominates the height fall of the MFC. While the lower-level thermal

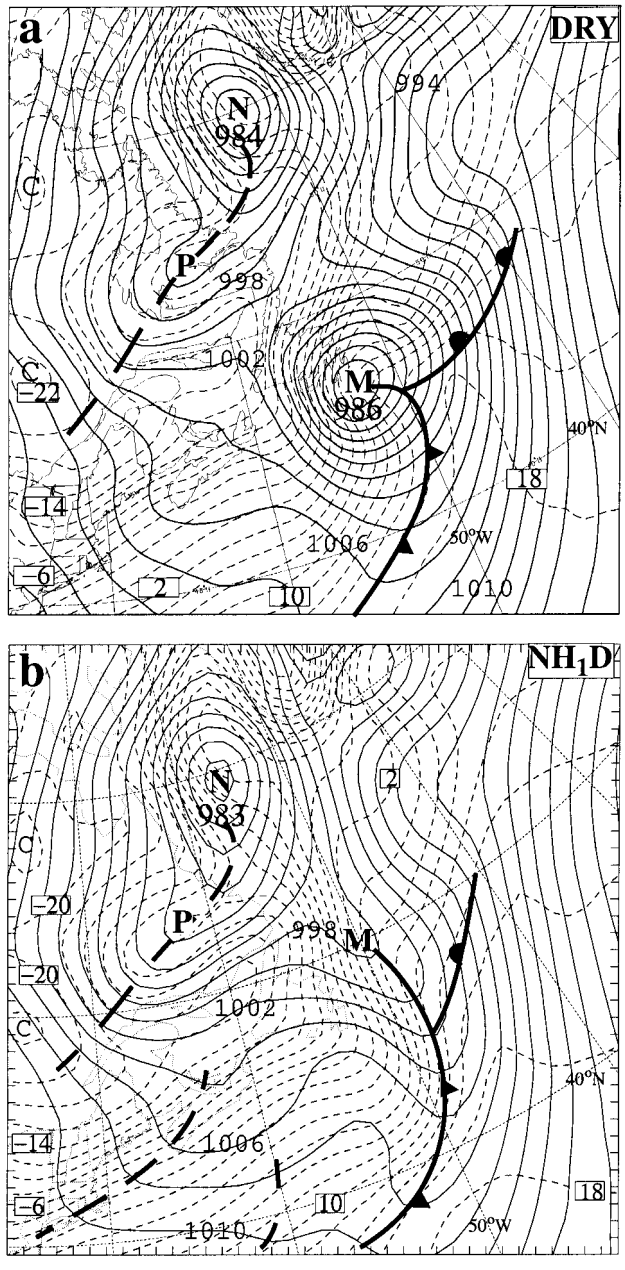

Figure 14. As in Fig. 1(c) but for experiments (a) DRY and (b) NH_1D at 00 UTC 15 March 1992 (see Table 5).

contribution is pronounced during the mature stage, it must be small and negligible prior to the MFC genesis. Thus, it is the Q_d-induced height fall associated with H_1 that helps trigger the low-level cyclonic circulation of the MFC. Because of the presence of the intense baroclinicity in the lowest layers, the thermal advection by the induced circulation increases with time, thereby amplifying the θ_{eff} anomaly in the vicinity of the cold-frontal zone (see Table 6). The sum of the height falls induced by the upper- and

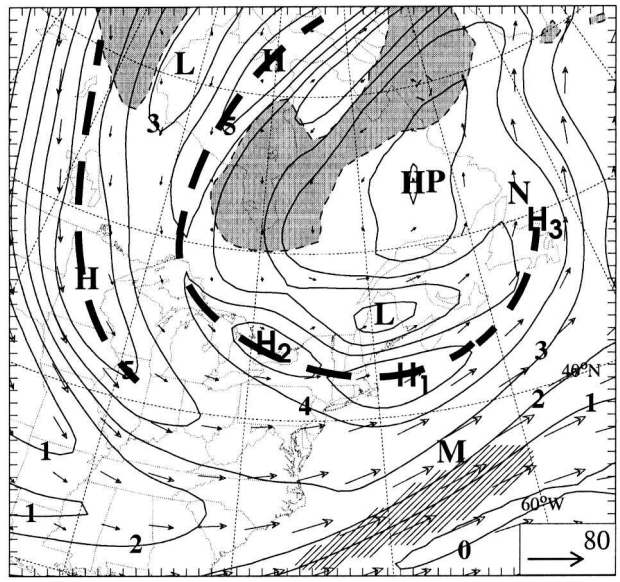

Figure 15. As in Fig. 2 but for experiment DRY at 00 UTC 14 March 1992 (see Table 5).

TABLE 6. AS IN TABLE 1 BUT FOR THE MAJOR FRONTAL CYCLONE IN EXPERIMENT DRY (SEE TABLE 5). NOTE THAT DIABATIC ATTRIBUTION IS EXCLUDED IN DRY.

Day/hour	Q_d+Q_r dam (%)	θ_{eff} dam (%)	Total (dam) dam
13/00	−3.9 (27.5)	−10.3 (72.5)	−14.2
13/12	−2.6 (25.5)	−7.6 (74.5)	−10.2
14/00	−3.8 (22.9)	−12.8 (77.1)	−16.6
14/12	−7.4 (31.5)	−16.1 (68.5)	−23.5
15/00	−11.7 (31.5)	−25.5 (68.5)	−37.2
15/12	−19.1 (46.7)	−21.8 (53.3)	−40.9

low-level anomalies exhibits a baroclinically favourable westward tilt; its circulation is about 200 hPa shallower than the moist one (cf. Figs. 16(c) and 5(h)).

(*b*) *Role of the PV perturbation H_1 in the MFC genesis*

We have shown in section 4 that the MFC is more sensitive to the PV perturbation H_1 than other PV perturbations (i.e. H_2 and H_3). Since the model's sensitivity is masked by latent-heat release in experiment NH_1, it is desirable to conduct another ('cleaner') experiment in which everything is identical to experiment DRY except that the H_1 perturbation is removed from the model initial conditions (experiment NH_1D). Without the H_1 perturbation, the dry dynamics could only produce a weak trough associated with the MFC by 15/00-48 (see Fig. 14(b)). Although this trough continues to drop its minimum pressure due to its being influenced by the PV reservoir in the upper-level outer ring, it fails to form a closed isobar even at the end of the 60 h integration (not shown). In the absence of an intense MFC, the NFC becomes deeper than that in experiment DRY and it eventually absorbs the parent circulation, as occurs in experiment N2H (Fig. 14(b)).

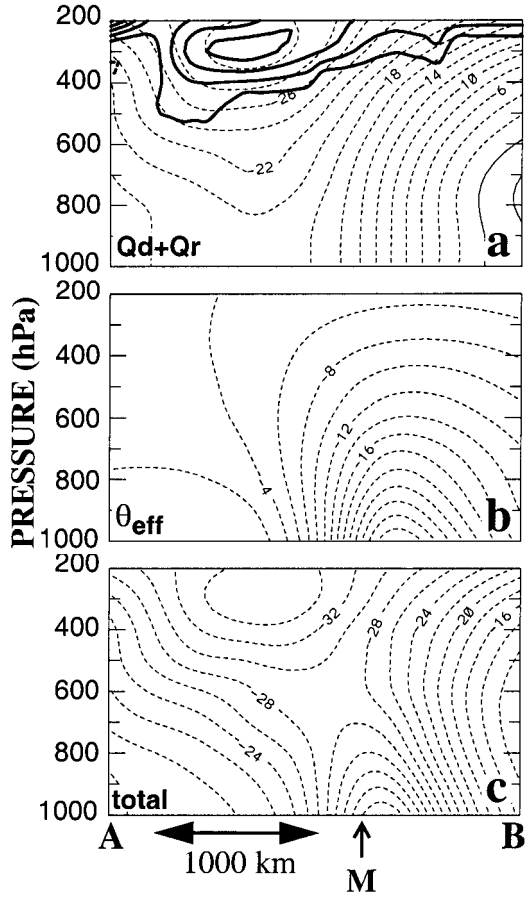

Figure 16. As in Fig. 5 but for experiment DRY at 00 UTC 15 March 1992 which is shown in a fashion similar to the right panel in Fig. 5.

An examination of the upper-level PV maps reveals a scenario similar to that shown in experiment NH_1 (see Fig. 13(a)); namely, the MFC is located far away to the south of the inner PV ring during the incipient stage. This reduced upper-level influence could be seen from Table 7, which shows the reduced contributions from Q_d+Q_r compared with those in experiment DRY except at 14/12-36 (cf. Tables 6 and 7). Of interest is that the low-level θ_{eff} contribution is also reduced significantly, e.g. compare -136 m in NH_1D with -218 m in DRY at 15/00-48. This reveals again the important role of the upper-level PV anomaly H_1 in facilitating the lower-level baroclinic conversion processes. That is, the H_1-induced low-level cyclonic circulation helps generate a favourable thermal advection pattern (i.e. warm ahead and cold behind), thereby leading to the amplification of the bottom effective thermal anomaly and the deepening of the MFC. The results indicate that in the present case *without any pronounced perturbation in the upper-level PV rings, the frontal cyclogenesis is not likely to take place even in the presence of intense low-level baroclinicity*.

This important influence of H_1 on the lower-level development could be demonstrated using Fig. 17, which compares the 900 hPa thermal advection as induced by all the flows (i.e. Q_d+Q_r, θ_{eff}, and mean) during the incipient stage of the MFC between experiments NH_1D and DRY. Of significance is that the H_1-induced winds at

TABLE 7. AS IN TABLE 6 BUT FOR THE MAJOR FRONTAL CYCLONE IN EXPERIMENT NH_1D (SEE TABLE 5)

Day/hour	Q_d+Q_r dam (%)	θ_{eff} dam (%)	Total (dam) dam
13/00	−1.3 (10.9)	−10.6 (89.1)	−11.9
13/12	−2.2 (32.8)	−4.5 (67.2)	−6.7
14/00	−2.3 (22.1)	−8.1 (77.9)	−10.4
14/12	−9.5 (57.2)	−7.1 (42.8)	−16.6
15/00	−11.7 (46.2)	−13.6 (53.8)	−25.3
15/12	−13.8 (64.2)	−7.7 (35.8)	−21.5

900 hPa are as strong as 15 m s^{-1} (Fig. 17(a)). Since the surface warmth is determined by the thermal gradient and the normal component of the induced flow with respect to the leading baroclinic zone, the H_1-induced cyclonic circulation tends to build up a warm anomaly centred at the MFC (Fig. 17(a)). The ensuing warmth would clearly help intensify the θ_{eff} anomaly causing the MFC's deepening. On the other hand, the θ_{eff}-induced cyclonic winds at 900 hPa tend to produce a cold anomaly in the south-west quadrant of the MFC (Fig. 17(c)), owing to the presence of large height gradients behind the cold-frontal zone (see Figs. 5(e) and (f) and 16(b)). Similarly, the thermal advection by the background flow, which is more associated with the parent cyclone, contributes negative tendencies to the 900 hPa thermal perturbation (Fig. 17(e)). It is apparent that the summation of all the PV anomaly-induced contributions would form a warm (cold) anomaly in the north-east (south-west) quadrant that is similar to the local pressure pattern shown in Figs. 5(e) and (f) and 16(b).

When H_1 is removed, the thermal advection pattern differs markedly in the vicinity of the MFC except for that induced by the background flow. In particular, the upper-level PV anomaly-induced cyclonic circulation is very weak, so is the warm advection (and θ_{eff}) in the vicinity of the MFC (Fig. 17(b)). *The weak thermal advection is essentially caused by the lack of an across-isothermal component of the induced circulation* (i.e. associated with a PV anomaly), as can be seen from the inverted flow vectors around the MFC (cf. Figs. 17(a) and (b)). The resulting weak perturbation θ_{eff} in NH_1D produces correspondingly weak thermal advection at 900 hPa (Fig. 17(d)). As a result, little bottom dynamical forcing is present for the MFC genesis in experiment NH_1D (Fig. 14(b)).

At this point, it is of interest to mention a recent study by Ziemiański and Thorpe (2000), who extended the conceptual model of Hoskins *et al.* (1985) by deriving the attribution of vertical motion to various PV anomalies within the nonlinear balanced-equation framework. They showed that the vertical motion induced by the low-level PV anomalies could contribute to the process of tropopause folding, leading to a strong coupling of the low- and upper-level flows. Clearly, the same attribution concept could be applied to the low- and upper-level interactions, leading to the surface frontal cyclogenesis in the present case.

Therefore, based on the results from experiments DRY and NH_1D, we may state that the PV anomaly associated with H_1 accounts for the triggering, and part of the subsequent deepening, of the MFC. This PV anomaly does not seem to have direct impact on the genesis of other frontal cyclones, but some indirect effects on their final intensity through the vortex–vortex interaction. *While the low-level thermal anomaly θ_{eff} accounts for a large portion of the deepening of the frontal cyclones, it is the upper-level PV anomalies that provide the necessary forcing for the amplification of θ_{eff} and the frontal cyclogenesis*.

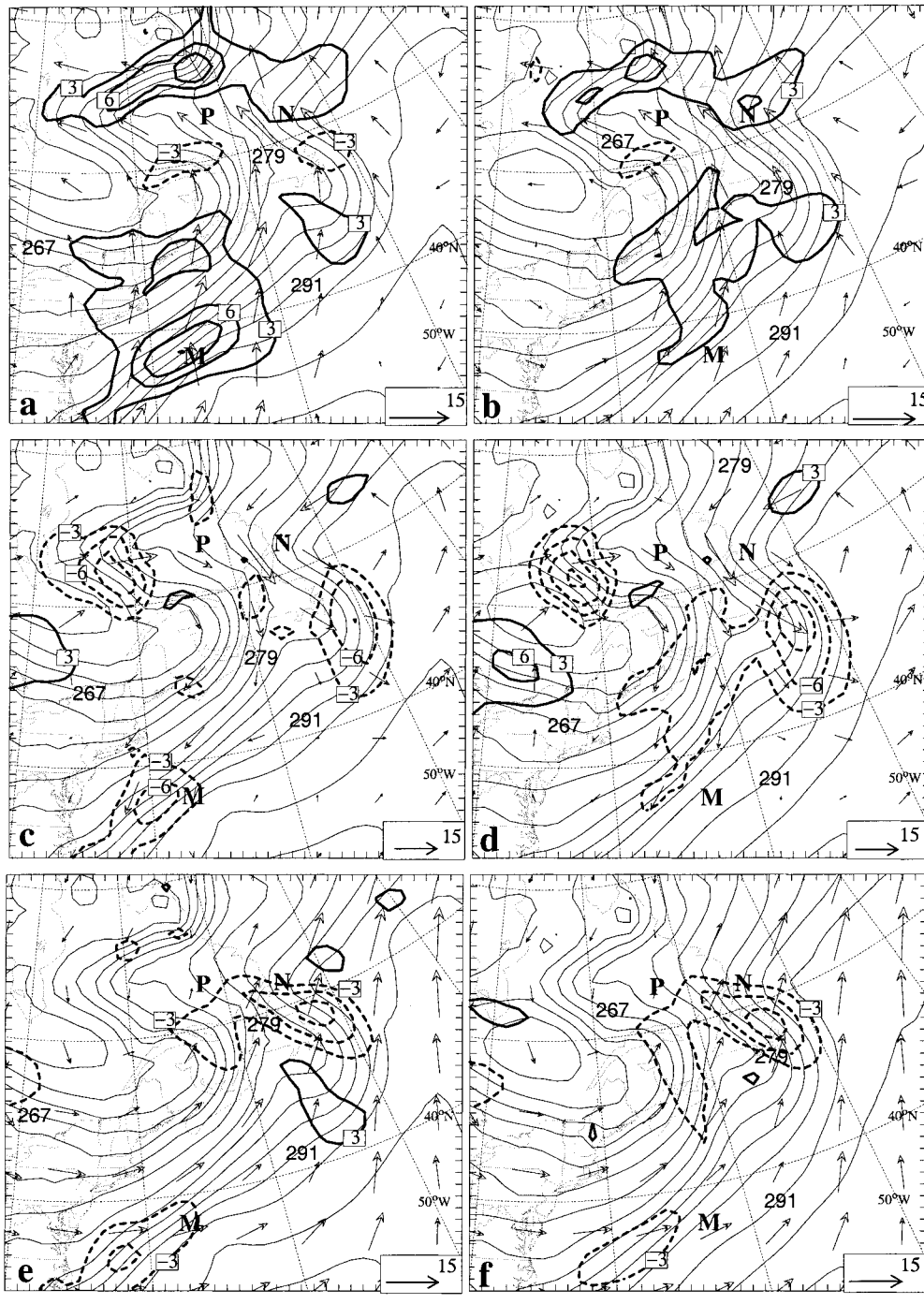

Figure 17. Horizontal distribution of the 900 hPa potential-temperature advection (thick) at intervals of 3 K (6 h)$^{-1}$ by the inverted winds from (a) and (b): upper-level dry-plus-residual potential vorticity (PV) anomalies, Q_d+Q_r; (c) and (d): effective bottom potential-temperature anomaly, θ_{eff}; (e) and (f): background state at 00 UTC 14 March 1992. Solid (dashed) lines denote positive (negative) values. Left and right panels are from experiments DRY and NH_1D, respectively (see Table 5). They are superposed with potential temperature (thin) at intervals of 3 K and the inverted wind vectors whose scales (m s^{-1}) are given in the insets.

6. Concluding remarks

In this study, the tracks and evolution of a family of frontal cyclones in relation to upper-level PV anomalies are examined through PV diagnostics, static piecewise PV inversion, and sensitivity simulations to removed PV anomalies. This is achieved by using 60 h simulations of six frontal cyclones that occurred over the western Atlantic between 0000 UTC 13 March and 1200 UTC 15 March 1992. More detailed analyses are performed for a major frontal cyclone because of its rapid deepening and robust circulation. It is shown that the tracks of the cyclone family follow closely the distribution of two (inner and outer) PV rings on the cyclonic-shear side of an upper-level jet stream, while the surface cyclogenesis occurs in the trailing frontal zone of a parent polar cyclone and in close proximity to propagating PV anomalies in the central portion of an upper-level parent trough. As each cyclone deepens, significant low-level PV anomalies develop as a result of latent-heat release. The diabatically generated PV anomaly in the MFC is well 'phase-locked' with the PV reservoir in the upper-level outer PV ring.

The static PV inversion diagnostics reveal that the bottom effective thermal anomaly (θ_{eff}) or the low-level thermal advection contributes the most to the MFC's and NFC's depths, followed by latent-heat release (Q_h), and upper-level PV anomalies (Q_d+Q_r), except near the end of the 60 h simulation when the MFC absorbs the NFC and parent circulations. The relative contribution of Q_d+Q_r decreases during the intensifying stages as a result of the increasing influence of the upper-level ridge to the east. In contrast, Q_d+Q_r contributes the most to the depth of the SFC and other three weaker frontal cyclones, followed by nearly equal contributions from Q_h and θ_{eff} during their incipient stages. It is speculated, however, that the θ_{eff} contributions would increase with time as these four frontal cyclones move into the ridge region ahead, just as occurred with the MFC and NFC.

Four sensitivity simulations are conducted to explore the influences of three major PV anomalies in the upper-level inner PV ring on the MFC genesis by removing each, or two of them, at a time from the control initial conditions and then integrating the model for 60 h. Removal of the three PV anomalies individually leads to different solutions in the track and intensity of the MFC. Specifically, removing a nearby PV anomaly (i.e. H_3) and an anomaly far upstream (i.e. H_2) causes little change in the MFC development. However, when a PV anomaly associated with a short-wave trough upstream (i.e. H_1) is removed, it produces a significant impact on the MFC development, namely, delaying its genesis by 18 h and weakening its final depth by 13 hPa. The most pronounced changes occur when H_1 and H_2 are both removed; it results in a delay of the MFC genesis by 36 h and a weakening of 21 hPa in central pressure. It is shown that *the MFC genesis during the first 36 h integration depends on PV perturbations in the inner PV ring, whereas its subsequent development depends more on the PV reservoir in the outer PV ring*. The results suggest that frontal cyclogenesis is less likely to occur on the anticyclonic-shear side of the upper-level jet stream unless other forcing mechanisms dominate (e.g. latent-heat release, and surface fluxes).

A sensitivity simulation, in which latent-heat release is excluded from the control run, confirms the critical roles of the upper-level PV anomalies in determining the tracks and genesis of the frontal-cyclone family. More significantly, the MFC fails to form a closed circulation even near the end of the 60 h integration, when the PV anomaly H_1 is removed. This is attributed to the lack of significant low-level thermal advection in the vicinity of the MFC as induced by this PV anomaly. This dry simulation suggests that even though the bottom thermal anomalies play an important role in deepening the frontal cyclones, it is the upper-level PV anomalies that provide the necessary forcing for its amplification leading to the frontal cyclogenesis.

In conclusion, we may state that propagating PV anomalies on the cyclonic side of the upper-level jet stream tend to induce low-level cyclonic circulations superposed on the leading baroclinic zone, a scenario similar to the conceptual model of Hoskins *et al.* (1985) in which cyclogenesis occurs when a positive upper-level PV anomaly overruns a low-level baroclinic zone. This result confirms the previous finding that the cyclonic-shear side of an upper-level jet stream is a favourable location for frontal cyclogenesis (Mullen 1979, 1982; Reed 1979). In particular, the development of *the multiple frontal cyclones* in the present case can be related closely to *the multiple propagating PV anomalies* in the two upper-level PV rings. Once the induced cyclonic circulations approach the cold-frontal zone in sequence, favourable thermal advection will result in the growth of successive bottom thermal anomalies, thereby leading to the spin-up of a family of frontal cyclones. These results appear to have important implications with respect to many cases of frontal cyclogenesis occurring during FASTEX.

ACKNOWLEDGEMENTS

This work was supported by National Science Foundation (NSF) grant ATM-9802391, National Aeronautics and Space Administration grant NAG-57842 and the National Science and Engineering Research Council of Canada. The computations were performed at the National Center for Atmospheric Research, which is sponsored by the NSF.

REFERENCES

Baehr, C., Pouponneau, B., Ayrault, F. and Joly, A. 1999 Dynamical characterization of the FASTEX cyclogenesis cases. *Q. J. R. Meteorol. Soc.*, **125,** 3469–3494

Bishop, C. H. and Thorpe, A. J. 1994 Frontal wave stability during moist deformation frontogenesis. Part I: Linear wave dynamics. *J. Atmos. Sci.*, **51,** 852–873

Bjerknes, J. and Solberg, H. 1922 Life cycle of cyclones and the polar front theory of atmospheric circulation. *Geophys. Publ.*, **3,** (1), 1–18

Bouniol, D., Protat, A. and Lemaître, Y. 1999 Mesoscale dynamics of a deepening secondary cyclone in FASTEX IOP16: Three-dimensional structure retrieved from dropsonde data. *Q. J. R. Meteorol. Soc.*, **125,** 3535–3562

Boyle, J. S. and Bosart, L. F. 1986 Cyclone–anticyclone couplets over North America. Part II: Analysis of a major cyclone event over the eastern United States. *Mon. Weather Rev.*, **114,** 2432–2465

Carrera, M. L., Gyakum, J. R. and Zhang, D.-L. 1999 A numerical case study of secondary marine cyclogenesis sensitivity to initial error and varying physical processes. *Mon. Weather Rev.*, **127,** 641–660

Davis, C. A. and Emanuel, K. A. 1991 Potential vorticity diagnostics of cyclogenesis. *Mon. Weather Rev.*, **119,** 1929–1953

Davis, C. A., Stoelinga, M. T. and Kuo, Y.-H. 1993 The integrated effect of condensation in numerical simulations of extratropical cyclogenesis. *Mon. Weather Rev.*, **121,** 2309–2330

Demirtas, M. and Thorpe, A. J. 1999 Sensitivity of short-range weather forecasts to local potential vorticity modifications. *Mon. Weather Rev.*, **127,** 922–939

Fehlmann, R. and Davies, H. C. 1999 Role of salient potential-vorticity elements in an event of frontal-wave cyclogenesis. *Q. J. R. Meteorol. Soc.*, **125,** 1801–1824

Hakim, G. J., Keyser, D. and Bosart, L. F. 1996 The Ohio Valley wave-merger cyclogenesis event of 25–26 January 1978. Part II: Diagnosis using quasigeostrophic potential vorticity inversion. *Mon. Weather Rev.*, **124,** 2176–2205

Hoskins, B. J., McIntyre, M. E. and Robertson, A. W. 1985 On the use and significance of isentropic potential vorticity maps. *Q. J. R. Meteorol. Soc.*, **111,** 877–946

Huo, Z., Zhang, D.-L. and Gyakum, J. R. 1996 The life cycle of the intense IOP-14 storm during CASP II. Part I: Analysis and simulations. *Atmos.-Ocean*, **34,** 51–80

1999a Interaction of potential vorticity anomalies in extratropical cyclogenesis. Part I: Static piecewise inversion. *Mon. Weather Rev.*, **127,** 2546–2561

Huo, Z., Zhang, D.-L. and Gyakum, J. R. 1999b Interaction of potential vorticity anomalies in extratropical cyclogenesis. Part II: Sensitivity to initial perturbations. *Mon. Weather Rev.*, **127,** 2563–2575

Joly, A. and Thorpe, A. J. 1990 Frontal instability generated by tropospheric potential vorticity anomalies. *Q. J. R. Meteorol. Soc.*, **116,** 525–560

Joly, A., Jorgensen, D., Shapiro, M. A., Thorpe, A., Bessemoulin, P., Browning, K. A., Cammas, J.-P., Chalon, J.-P., Clough, S. A., Emanuel, K. A., Eymard, L., Gall, G., Hildebrand, P. H., Langland, R. H., Lemaître, Y., Lynch, P., Moore, J. A., Persson, P. O. G., Snyder, C. and Wakimoto, R. M. 1997 The Fronts and Atlantic Storm-Track EXperiment (FASTEX): Scientific objectives and experimental design. *Bull. Am. Meteorol. Soc.*, **78,** 1917–1940

Joly, A., Browning, K. A., Bessemoulin, P., Cammas, J.-P., Caniaux, G., Chalon, J.-P., Clough, S. A., Dirks, R., Emanuel, K. A., Eymard, L., Gall, R., Hewson, T. D., Hildebrand, P. H., Jorgensen, D., Lalaurette, F., Langland, R. H., Lemaître, Y., Mascart, P., Moore, J. A., Persson, P. O. G., Roux, F., Shapiro, M. A., Snyder, C., Toth, Z. and Wakimoto, R. M. 1999 Overview of the field phase of the Fronts and Atlantic Storm-Track EXperiment (FASTEX) project. *Q. J. R. Meteorol. Soc.*, **125,** 3131–3164

Kuo, Y.-H. and Reed, R. J. 1988 Numerical simulation of an explosively deepening cyclone in the eastern Pacific. *Mon. Weather Rev.*, **116,** 2081–2105

Lapenta, W. M. and Seaman, N. L. 1992 A numerical investigation of east coast cyclogenesis during the cold-air damming event of 27–28 February 1982. Part II: Importance of physical mechanisms. *Mon. Weather Rev.*, **120,** 52–76

Lemaître, Y., Protat, A. and Bouniol, D. 1999 Pacific and Atlantic 'bomb-like' deepenings in the mature phase: A comparative study. *Q. J. R. Meteorol. Soc.*, **125,** 3513–3534

Lupo, A. R., Smith, P. J. and Zwack, P. 1992 A diagnosis of the explosive development of two extratropical cyclones. *Mon. Weather Rev.*, **120,** 1490–1523

Mallet, I., Arbogast, P., Baehr, C., Cammas, J. P. and Mascart, P. 1999 Effects of a low-level precursor and frontal stability on cyclogenesis during FASTEX IOP17. *Q. J. R. Meteorol. Soc.*, **125,** 3415–3438

Mullen, S. L. 1979 An investigation of small synoptic-scale cyclones in polar air streams. *Mon. Weather Rev.*, **107,** 1636–1647

1982 Cyclone development in polar air streams over the wintertime continent. *Mon. Weather Rev.*, **110,** 1664–1676

Newton, C. W. and Holopainen, E. O. 1990 *Extratropical cyclones. The Erik Palmén memorial volume.* Am. Meteorol. Soc.

Parker, D. J. 1998 Secondary frontal waves in the North Atlantic region: A dynamical perspective of current ideas. *Q. J. R. Meteorol. Soc.*, **124,** 829–856

Reed, R. J. 1979 Cyclogenesis in polar air streams *Mon. Weather Rev.*, **107,** 38–52

Reed, R. J., Kuo Y.-H. and Low-Nam, S. 1994 An adiabatic simulation of the ERICA IOP-5 storm. Part II: Sensitivity tests and further diagnosis based on model output. *Mon. Weather Rev.*, **121,** 1595–1612

Sanders, F. and Gyakum, J. R. 1980 Synoptic–dynamic climatology of the 'bomb'. *Mon. Weather Rev.*, **108,** 1589–1606

Schär, C. and Davies, H. C. 1990 An instability of mature cold fronts. *J. Atmos. Sci.*, **47,** 929–950

Shapiro, M. A. and Gronas, S. 1999 *The life cycles of extratropical cyclones.* Am. Meteorol. Soc.

Snyder, C. 1996 Summary of informal workshop on adaptive observations and FASTEX. *Bull. Am. Meteorol. Soc.*, **77,** 953–961

Thorncroft, C. D. and Hoskins, B. J. 1990 Frontal cyclogenesis. *J. Atmos. Sci.*, **47,** 2317–2337

Wang, J. and Zhang, D.-L. 2000 A case study of frontal cyclogenesis and its sensitivity to coastal initial conditions. *Acta Meteorol. Sinica*, **14,** 173–192

Whitaker, J. S., Uccellini, L. W. and Brill, K. F. 1988 A model-based diagnostic study of the rapid development stage of the Presidents' Day cyclone. *Mon. Weather Rev.*, **116,** 2337–2365

Zhang, D.-L., Radeva, E. and Gyakum, J. R. 1999a A family of frontal cyclones over the western Atlantic Ocean. Part I: A 60-h simulation. *Mon. Weather Rev.*, **127,** 1725–1744

1999b A family of frontal cyclones over the western Atlantic Ocean. Part II: Parameter studies. *Mon. Weather Rev.*, **127**, 1745–1760

Ziemiański, M. Z. and Thorpe, A. J. 2000 The dynamical consequences for tropopause folding of PV anomalies induced by surface frontal collapse. *Q. J. R. Meteorol. Soc.*, **126,** 2727–2764

Zwack, P. and Okossi, B. 1986 A new method for solving the quasigeostrophic omega equation by incorporating surface pressure tendency data. *Mon. Weather Rev.*, **114,** 655–666